
Learning Conditional Deformable Templates with Convolutional Networks

Adrian V. Dalca*
CSAIL, MIT
MGH, HMS

Marianne Rakic
D-ITET, ETH
CSAIL, MIT

John Guttag
CSAIL, MIT

Mert R. Sabuncu
ECE and BME, Cornell

Abstract

We develop a learning framework for building deformable templates, which play a fundamental role in many image analysis and computational anatomy tasks. Conventional methods for template creation and image alignment to the template have undergone decades of rich technical development. In these frameworks, templates are constructed using an iterative process of template estimation and alignment, which is often computationally very expensive. Due in part to this shortcoming, most methods compute a single template for the entire population of images, or a few templates for specific sub-groups of the data. In this work, we present a probabilistic model and efficient learning strategy that yields either universal or *conditional* templates, jointly with a neural network that provides efficient alignment of the images to these templates. We demonstrate the usefulness of this method on a variety of domains, with a special focus on neuroimaging. This is particularly useful for clinical applications where a pre-existing template does not exist, or creating a new one with traditional methods can be prohibitively expensive. Our code and atlases are available online as part of the VoxelMorph library at <http://voxelmorph.csail.mit.edu>.

Keywords. deformable templates, conditional atlases, diffeomorphic image registration, probabilistic models, neuroimaging

1 Introduction

A deformable template is an image that can be geometrically deformed to match images in a dataset, providing a common reference frame. Templates are a powerful tool that enables the analysis of geometric variability. They have been used in computer vision [26, 37, 42], medical image analysis [3, 21, 40, 50], graphics [44, 65], and time series signals [1, 72]. We are motivated by the study of anatomical variability in neuroimaging, where collections of scans are mapped to a common template with anatomical and/or functional landmarks. However, the methods developed here are applicable to other domains.

Analysis with a deformable template is often done by computing a smooth deformation field that *aligns* the template to another image. The deformation field can be used to derive a measure of the differences between the two images. Rapidly obtaining this field to a given template is by itself a challenging task and the focus of extensive research.

A template can be chosen as one of the images in a given dataset, but often these do not represent the structural variability and complexity in the image collection, and can lead to biased and misleading analyses [40]. If the template does not adequately represent dataset variability, such as the possible anatomy, it becomes challenging to accurately deform the template to some images. A good template

* adalca@mit.edu

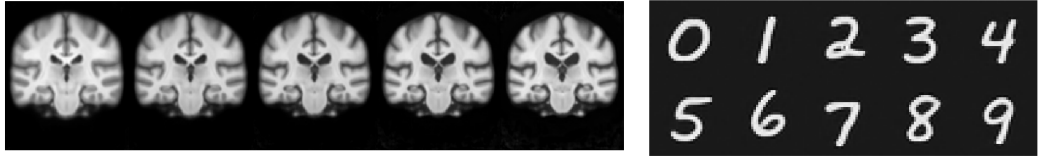


Figure 1: Conditional deformable templates generated by our method. Left: slices from 3D brain templates conditioned on age; Right: MNIST templates conditioned on class label.

therefore minimizes the geometric distance to all images in a dataset, and there has been extensive methodological development for finding such a central template [3, 21, 40, 50]. However, these templates are obtained through a costly global optimization procedure and domain-specific heuristics, requiring extensive runtimes. For complex 3D images such as MRI, this process can consume days to weeks. In practice, this leads to few templates being constructed, and researchers often use templates that are not optimal for their dataset. Our work makes it easy and computationally efficient to generate deformable templates.

While deformable templates are powerful, a single template may be inadequate at capturing the variability in a large dataset. Existing methods alleviate this problem by grouping subpopulations, usually along a single attribute, and computing separate templates for each group. This approach relies on arbitrary decisions about the attributes and thresholds used for subdividing the dataset. Furthermore, each template is only constructed based on a subset of the data, thus exploiting fewer images, leading to sub-optimal templates. Instead, we propose a learning-based approach that can compute on-demand *conditional* deformable templates by leveraging the entire collection. Our framework enables the use of multiple attributes, continuous (e.g., age) or discrete (e.g., sex), to condition the template on, without needing to apply arbitrary thresholding or subdividing a dataset.

We formulate template estimation as a learning problem and describe a novel method to tackle it.

- (1) We describe a probabilistic spatial deformation model based on diffeomorphisms. We then develop a general, end-to-end framework using convolutional neural networks that jointly synthesizes templates and rapidly provides the deformation field to any new image.
- (2) This framework also enables learning a *conditional* template function given instance attributes, such as the age and sex of the subject in an MRI. Once learned, this function enables rapid synthesis of on-demand conditional templates. For example, it could construct a 3D brain MRI template for 35 year old women.
- (3) We demonstrate the template construction method and its utility on a variety of datasets, including a large neuroimaging study. In addition, we show preliminary experiments indicating characteristics and interesting results of the model. For example, this formulation can be extended to learn image representations up to a deformation.

Conditional templates capture important trends related to attributes, and are useful for dealing with confounders. For example, in studying disease impact, for some tasks it may be helpful to register scans to age-specific templates rather than one covering a wide age range.

2 Related Works

2.1 Spatial Alignment (Image Registration)

Spatial alignment, or registration, between two images is a building block for estimation of deformable templates. Alignment usually involves two steps: a global affine transformation, and a deformable transformation (as in many optical flow applications). In this work we focus on, and make use of, deformable transformations.

There is extensive work in deformable image registration methods [5, 6, 7, 10, 19, 28, 67, 71, 73]. Conventional frameworks optimize a regularized dense deformation field that matches one image with the other [7, 67]. Diffeomorphic transforms are topology preserving and invertible, and have been widely used in computational neuroanatomy analysis [6, 5, 10, 13, 14, 32, 41, 55, 59, 69, 73]. While

extensively studied, conventional registration algorithms require an optimization for every pair of images, leading to long runtimes in practice.

Recently, learning based registration methods have been proposed that offer a significant speed-up at test time [8, 9, 12, 17, 18, 23, 47, 46, 61, 64, 70]. These methods learn a network that computes the deformation field, either in a supervised (using ground truth deformations), unsupervised (using classical energy functions), or semi-supervised setting. These algorithms have been used for registering an image to an *existing* template. However, in many realistic scenarios, a template is not readily available, for example in a clinical study that uses a particular scan protocol. We build on these ideas in our learning strategy, but jointly estimate a registration network and a conditional deformable template in an unsupervised setting.

Optical flow methods are closely related to image registration, finding a dense displacement field for a pair of 2D images. Similar to registration, classical approaches solve an optimization problem, often using variational methods [11, 35, 66]. Learning-based optical flow methods use convolutional neural networks to learn the dense displacement fields [2, 25, 36, 38, 60, 68].

2.2 Template Construction

Deformable templates, or *atlases*, are widely used in computational anatomy. Specifically, the deformation fields from this template to individual images are often carefully analyzed to understand population variability. The template is usually constructed through an iterative procedure based on a collection of images or volumes. First, an initial template is chosen, such as an example image or a pixel-wise average across all images. Next, all images are aligned (registered) to this template, a better template is estimated from aligned images through averaging, and the process is iterated until convergence [3, 21, 40, 50, 63]. Since the above procedure requires many iterations involving many costly (3D) pairwise registrations, atlas construction runtimes are often prohibitive.

A single population template can be insufficient at capturing complex variability. Current methods often subdivide the population to build multiple atlases. For example, in neuroimaging, some methods build different templates for different age groups, requiring rigid discretization of the population and prohibiting each template from using all information across the collection. Images can also be clustered and a template optimized for each cluster, requiring a pre-set number of clusters [63]. Specialized methods have also been developed that tackle a particular variability of interest. For example, spatiotemporal brain templates have been developed using specialized registration pipelines and explicit modelling of brain degeneration with time [22, 31, 48], requiring significant domain knowledge, manual anatomical segmentations, and significant computational resources. We build on the intuitions of these methods, but propose a general framework that can learn *conditional* deformable templates for any given set of attributes. Specifically, our strategy learns a single network that leverages shared information across the entire dataset and can output different templates as a function of sets of attributes, such as age, sex, and disease state. The conditional function learned by our model generates unbiased population templates for a specific configuration of the attributes.

Our model can be used to study the population variation with respect to certain attributes it was trained on, such as age in neuroimaging. In recent literature on deep probabilistic models, several papers find and explore *latent* axes of important variability in the dataset [4, 15, 30, 33, 43, 51]. Our model can also be used to build conditional geometric templates based on such *latent* information, as we show in our experiments. In this case, our model can be seen as learning meaningful image representations up to a geometric deformation. However, in this paper we focus on observed (measured) attributes, with the goal of explicitly capturing variability that is often a source of confounding.

3 Methods

We first present a generative model that describes the formation of images through deformations from an unknown conditional template. We present a learning approach that uses neural networks and diffeomorphic transforms to jointly estimate the global template and a network that rapidly aligns it to each image.

3.1 Probabilistic model

Let \mathbf{x}_i be a data sample, such as a 2D image, a 3D volume like an MRI scan, or a time series. For the rest of this section, we use images and volumes as an example, but the development applies broadly to many data types. We assume we have a dataset $\mathcal{X} = \{\mathbf{x}_i\}$, and model each image as a spatial deformation ϕ_{v_i} of a global template \mathbf{t} . Each transform ϕ_{v_i} is parametrized by the random vector \mathbf{v}_i .

We consider a model of a *conditional* template $\mathbf{t} = f_{\theta_t}(\mathbf{a})$, a function of attribute vector \mathbf{a} , parametrized by global parameters θ_t . For example, \mathbf{a} can encode a class label or phenotypical information associated with medical scans, such as age and sex. In the case where no such conditioning information is available or of interest, this formulation reduces to a standard single template for the entire dataset: $\mathbf{t} = \mathbf{t}_{\theta_t}$, where θ_t can represent the pixel intensity values to be estimated.

We estimate the deformable template parameters θ_t and the deformation fields for every data point using maximum likelihood. Letting $\mathcal{V} = \{\mathbf{v}_i\}$ and $\mathcal{A} = \{\mathbf{a}_i\}$,

$$\begin{aligned}\hat{\theta}_t, \hat{\mathcal{V}} &= \arg \max_{\theta_t, \mathcal{V}} \log p_{\theta_t}(\mathcal{V} | \mathcal{X}, \mathcal{A}) \\ &= \arg \max_{\theta_t, \mathcal{V}} \log p_{\theta_t}(\mathcal{X} | \mathcal{V}; \mathcal{A}) + \log p(\mathcal{V}),\end{aligned}\quad (1)$$

where the first term captures the likelihood of the data and deformations, and the second term controls a prior over the deformation fields.

Deformations. While the method described in this paper applies to a range of deformation parametrization \mathbf{v} , we focus on diffeomorphisms. Diffeomorphic deformations are invertible and differentiable, thus preserving topology. Specifically, we treat \mathbf{v} as a stationary velocity field [5, 17, 32, 45, 46, 57], although time-varying fields are also possible. In this setup, the deformation field ϕ_v is defined through the following ordinary differential equation:

$$\frac{\partial \phi_v^{(t)}}{\partial t} = \mathbf{v}(\phi_v^{(t)}), \quad (2)$$

where $\phi^{(0)} = Id$ is the identity transformation and t is time. We can obtain the final deformation field $\phi^{(1)}$ by integrating the stationary velocity field \mathbf{v} over $t = [0, 1]$. We compute this integration through *scaling and squaring*, which has been shown to be efficiently implementable in automatic differentiation platforms [18, 45].

We model the velocity field prior $p(\mathcal{V})$ to encourage desirable deformation properties. Specifically, we first assume that deformations are smooth, for example to maintain anatomical consistency. Second, we assume that population templates are unbiased, restricting deformation statistics. Letting \mathbf{u}_v be the spatial displacement for $\phi_v = Id + \mathbf{u}_v$, and $\nabla \mathbf{u}_v$ be its spatial gradient,

$$p(\mathcal{V}) \propto \exp\{-\gamma \|\bar{\mathbf{u}}_v\|^2\} \prod_i \mathcal{N}(\mathbf{u}_{v_i}; \mathbf{0}, \Sigma_u) \quad (3)$$

where $\mathcal{N}(\cdot; \mu, \Sigma)$ is the multivariate normal distribution with mean μ and covariance Σ , and $\bar{\mathbf{u}}_v = 1/n \sum_i \mathbf{u}_{v_i}$. We let $\Sigma^{-1} = \mathbf{L}$, where $\mathbf{L} = \lambda_d \mathbf{D} - \lambda_a \mathbf{C}$ is (a relaxation of) the Laplacian of a neighborhood graph defined on the pixel grid, with the graph degree matrix \mathbf{D} and the pixel neighbourhood adjacency matrix \mathbf{C} [17]. Using this formulation, we obtain

$$\log p(\mathcal{V}) = -\gamma \|\bar{\mathbf{u}}_v\|^2 - \sum_i \frac{d}{2} \lambda_d \|\mathbf{u}_{v_i}\|^2 + \sum_i \frac{\lambda_a}{2} \|\nabla \mathbf{u}_{v_i}\|^2 + \text{const} \quad (4)$$

where d is the neighbourhood degree. The first term encourages a small *average* deformation across the dataset, encouraging a central, unbiased template. The second and third terms encourage templates that minimize deformation size and smoothness, respectively, and γ , λ_d and λ_a are hyperparameters.

Data Likelihood. The data likelihood $p(\mathbf{x}_i | \mathbf{v}_i, \mathbf{a}_i)$ can be adapted to the application domain. For images, we often adopt a simple additive Gaussian model coupled with a deformable template:

$$p(\mathbf{x}_i | \mathbf{v}_i; \mathbf{a}_i) = \mathcal{N}(\mathbf{x}_i; f_{\theta_t}(\mathbf{a}_i) \circ \phi_{v_i}, \sigma^2 \mathbb{I}), \quad (5)$$

where \circ represents a spatial warp, and σ^2 represents additive image noise. However, in some datasets, different likelihoods are more appropriate. For example, due to the spatial variability of contrast and noise in MRIs, likelihood models that result in normalized cross correlation loss functions have been widely shown to lead to more robust results, and such models can be used with our framework [6].

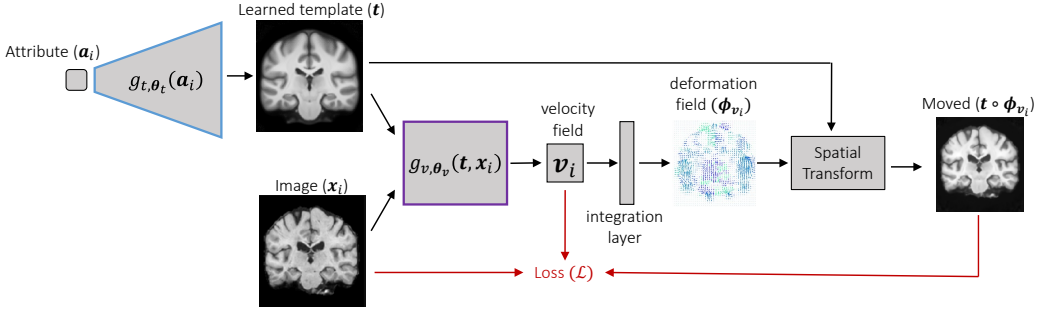


Figure 2: **Overview.** The network takes as input an image and an optional attribute vector. The upper network $g_{t, \theta_t}(\cdot)$ outputs a template, which is then registered with the input image by the second network $g_{v, \theta_v}(\cdot)$. The loss function, derived from the negative log likelihood of the generative model, leverages the template warped into $\mathbf{t} \circ \phi_{\mathbf{v}_i}$.

3.2 Neural Network Model

To solve the maximum likelihood formulation (1) given the model instantiations specified above, we design a network $g_{\theta}(\mathbf{x}_i, \mathbf{a}_i) = (\mathbf{v}_i, \mathbf{t})$ that takes as input an image and an attribute vector to condition the template on (this could be empty for global templates). The network can be effectively seen as having two functional parts. The first, $g_{t, \theta_t}(\mathbf{a}_i) = \mathbf{t}$, produces the conditional template. The second, $g_{v, \theta_v}(\mathbf{t}, \mathbf{x}_i) = \mathbf{v}_i$, takes in the template and a data point, and outputs the most likely velocity field (and hence deformation) between them. By learning the optimal parameters $\hat{\theta} = \{\hat{\theta}_t, \hat{\theta}_v\}$, we estimate a global network that simultaneously provides a deformable (conditional) template and its deformation to a datapoint. Figure 2 provides an overview schematic of the proposed network.

We optimize the neural network parameters θ using stochastic gradient algorithms, and minimize the negative maximum likelihood (1) for image \mathbf{x}_i :

$$\begin{aligned} \mathcal{L}(\theta_t, \theta_v; \mathbf{v}_i, \mathbf{x}_i, \mathbf{a}_i) &= -\log p_{\theta}(\mathbf{v}_i, \mathbf{x}_i; \mathbf{a}_i) \\ &= -\log p_{\theta}(\mathbf{x}_i | \mathbf{v}_i; \mathbf{a}_i) - \log p_{\theta}(\mathbf{v}_i) \\ &= -\frac{1}{2\sigma^2} \|\mathbf{x}_i - g_{t, \theta_t}(\mathbf{a}_i) \circ \phi_{\mathbf{v}_i}\|^2 - \gamma \|\bar{\mathbf{u}}\|^2 - \lambda_d \frac{d}{2} \sum_i \|\mathbf{u}_i\|^2 + \frac{\lambda_a}{2} \sum_i \|\nabla \mathbf{u}_i\|^2 + \text{const}, \quad (6) \end{aligned}$$

where $g_{t, \theta_t}(\mathbf{a}_i)$ yields the template at iteration i , and $\mathbf{v}_i = g_{v, \theta_v}(\mathbf{t}_{\theta_t, i}, \mathbf{x}_i)$.

The use of stochastic gradients to update the networks enables us to learn templates faster than conventional methods by avoiding the need to compute final deformations at each iteration. Intuitively, with every iteration the network learns to output a template, optionally conditioned on the attribute data, that can be smoothly and invertably warped to every image in the dataset.

We implement the template network $g_{t, \theta_t}(\cdot)$ with two versions, depending on whether we are estimating an unconditional or conditional template. The first, conditional version $g_{t, \theta_t}(\mathbf{a}_i)$ consists of a decoder that takes as input the attribute data \mathbf{a}_i , and outputs the template \mathbf{t} . The decoder includes a fully connected layer, followed by several blocks of upsampling, convolutional, and ReLU activation layers. The second, unconditional version g_{t, θ_t} has no inputs and simply consists of a learnable parameter at each pixel. The registration network $g_{v, \theta_v}(\mathbf{t}, \mathbf{x}_i)$ takes as input two images \mathbf{t} and \mathbf{x}_i and outputs a stationary velocity field \mathbf{v}_i , and is designed as a convolutional U-Net like architecture [62] with the design used in recent registration literature [9]. To compute the loss (6), we compute the deformation field $\phi_{\mathbf{v}_i}$ from \mathbf{v}_i using differentiable scaling and squaring integration layers [17, 45], and the warped template $\mathbf{t} \circ \phi_{\mathbf{v}_i}$ using spatial transform layers. We approximate the average deformation $\bar{\mathbf{u}}$ in the loss function using a weighted running average $\bar{\mathbf{u}} \sim \sum_{k=K-c}^K \mathbf{u}_k$, where \mathbf{u}_k is the displacement at iteration k , K is the current iteration, and c is usually set to 100 in our experiments. Specific network design parameters depend on the application domain, and are included in the supplementary materials.

3.3 Test-time Inference of Template and Deformations.

Given a trained network, we obtain a (potentially conditional) template \hat{t} directly from network $g_{t, \theta_t}(\mathbf{a}_i)$ by a single forward pass given input \mathbf{a}_i . For each test input image \mathbf{x}_i , the deformation fields themselves are often of interest for analysis or prediction. The network also provides the deformation $\hat{\phi}_{\hat{v}_i}$, where $\hat{v}_i = g_{v, \theta_v}(\hat{t}, \mathbf{x}_i)$.

Often times, the inverse deformation, which takes the image to the template space, is also desired. Using a stationary velocity field representation, obtaining this inverse deformation ϕ_v^{-1} is easy to compute by integrating the negative velocity field using the same scaling and squaring layer: $\phi_v^{-1} = \phi_{-v}$ [5, 18, 56].

4 Experiments

We present two main sets of experiments. The first set uses image-based datasets MNIST and Google QuickDraw, with the goal of providing a picture of the capabilities of our method. While deformable templates in these data are not a real-world application, these are often-studied datasets that provide a platform to analyze aspects of deformable templates.

In contrast, the second set of experiments is designed to demonstrate the utility of our method on a task of practical importance, analysis of brain MRI. We demonstrate that our method can produce high quality deformable templates in the context of realistic data, and that conditional deformable templates capture important anatomical variability related to age.

4.1 Experiment on Benchmark Datasets

Data. We use the MNIST dataset, consisting of small 2D images of hand-written digits [49] and 11 classes from the Google QuickDraw dataset [39], a collection of categorized drawings contributed by players in an online drawing game. To evaluate our method’s ability to construct conditional templates that accurately capture the impact of the variables on which the templates are conditioned, we generate examples in which the initial images are scaled and rotated (Figure 3). Specifically, we use an image scaling factor in the range 0.7 – 1.3 and an image rotation in the range 0 to 360 degrees. We learn different models involving either the original dataset involving different classes (D-class), the dataset with simulated scale effects (D-class-scale), and the rotations (D-class-scale-rot). While simulated image changes are obvious to an observer, during training we assume we know the attributes that cause changes in the images, but do not *a priori* model their effect on the images. This simulates, for example, the correlation between age and changing size of anatomical structures. The goal is to understand whether the proposed method is able to *learn* the relationship between the attribute and the geometrical variability in the dataset, and therefore produce a function for generating on-demand templates conditioned on the attributes. The datasets are split into train, validation and test sets.

4.1.1 Validation

In the first experiment, we evaluate our ability to construct suitable conditional templates.

Hyperparameters. Model hyperparameters have intuitive effects on the sharpness of the templates, the spatial smoothness of the registration fields, and the quality of the alignments. In practical settings, they should be chosen based on the desired goal of a given task. In these experiments, we tune hyperparameters by visually assessing deformations on validation data, starting from $\gamma = 0.01$, $\lambda_d = 0.001$, $\lambda_a = 0.01$, and $\sigma = 1$ for training on the D-class data. We found that once a hyperparameter was chosen for one dataset, only minor tuning was required for other experiments.

Evaluation criteria. Template construction is an ill-posed problem, and the utility of resulting templates depends on the desired task. We report a series of measures to capture properties of the resulting templates and deformations. Our first two quantitative evaluation criteria relate to centrality, for which we computed the norm of the mean displacement field $\|\bar{\mathbf{u}}\|^2$ and the average displacement size $\frac{1}{n} \sum_i \|\mathbf{u}_i\|^2$. Next, we illustrate field regularity per image class, and average intensity image agreement (via MSE). These metrics capture aspects about the deformation fields, rather than solely

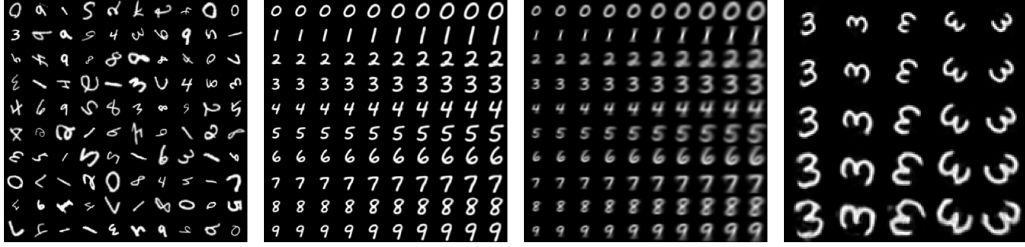


Figure 3: **MNIST examples** (1) MNIST digits from D-scale-rot; (2) templates conditioned on class (vertical axis) and scale (horizontal axis) on MNIST D-scale, learned with our model, and (3) with a decoder-only baseline model; (4) conditional templates learned with our model on the MNIST D-class-scale-rot dataset for the digit 3 and a variety of scaling and rotation values.

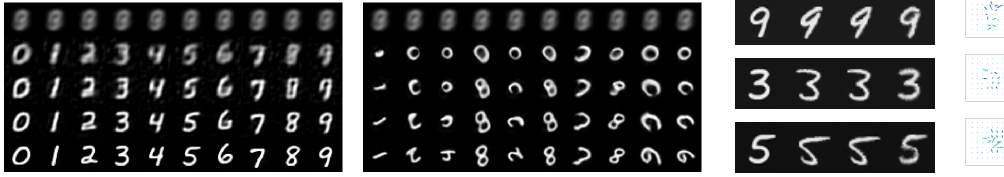


Figure 4: **Example convergence.** Convergence of two conditional template models. Left: model trained on digit-only attribute on D-class for epochs [0, 1, 2, 5, 100]. Right: model trained on D-class-rot, with all three attributes given as input to the model for epochs [0, 50, 75, 150, 1020], and randomly sampled digits [1, 2, 4, 8, 2, 8, 7, 8, 6, 6], rotations, and scales.

Figure 5: **Example deformations.** Each row shows: class template, example class image, template *warped* to this instance, instance *warped* to match the template, and the deformation field.

intrinsic properties of the templates. They need to be evaluated together - otherwise, deformation fields can lead to perfectly matching the image and template while being very irregular and geometrically meaningless, or can be perfectly smooth (zero displacement) at the cost of poor image matching. To capture field regularity, we compute the Jacobian matrix $J_\phi(p) = \nabla \phi(p) \in R^{3 \times 3}$, which captures the local properties of ϕ around voxel pixel p . Low values indicate irregular deformation fields, and $|J_\phi(p)| \leq 0$ indicate pixels that are not topology-preserving. Jacobian determinants near 1 represent very smooth fields. We use held-out test subjects for these measures.

Baselines. We compare our templates with templates built by choosing exemplar data as templates, and by training only a decoder of the given attributes using MSE loss and the same network architecture as the template network $g_{t, \theta_t}(\cdot)$. This latter baseline can be seen as differing from our method in that it minimizes a pixel-wise intensity difference as opposed to a geometric difference (deformation).

Results. Figure 3 illustrates conditional templates using our model and the decoder, and results from our model on the full MNIST dataset using all attributes. Our method produces sharp, central templates that are plausible digits and are smoothly deformable to other digits. Example deformations are shown in Figure 5. Supplementary Figures 14 contains similar results for the QuickDraw dataset.

Figure 4 illustrates convergence behavior for two models, showing that the conditional attributes are able to capture complicated geometric differences. Templates early in the learning process share appearance features across attributes, indicating that the network leverages common information across the dataset. The final templates enable significantly smaller deformations than early ones, indicating better representation of the conditional variability. As one would expect, more epochs are necessary for convergence of the model with more attributes.

Figure 6 shows template measures indicating that our conditional templates are more central and require smaller deformations than the baselines when registered with the test set digits. In Figure 6 we also find that our method and exemplar-based templates can perform well for both deformation metrics, and comparable to each other. Specifically, all deformations are "smooth" (no negative Jacobian determinants are detected) and image differences are visually imperceptible. We underscore

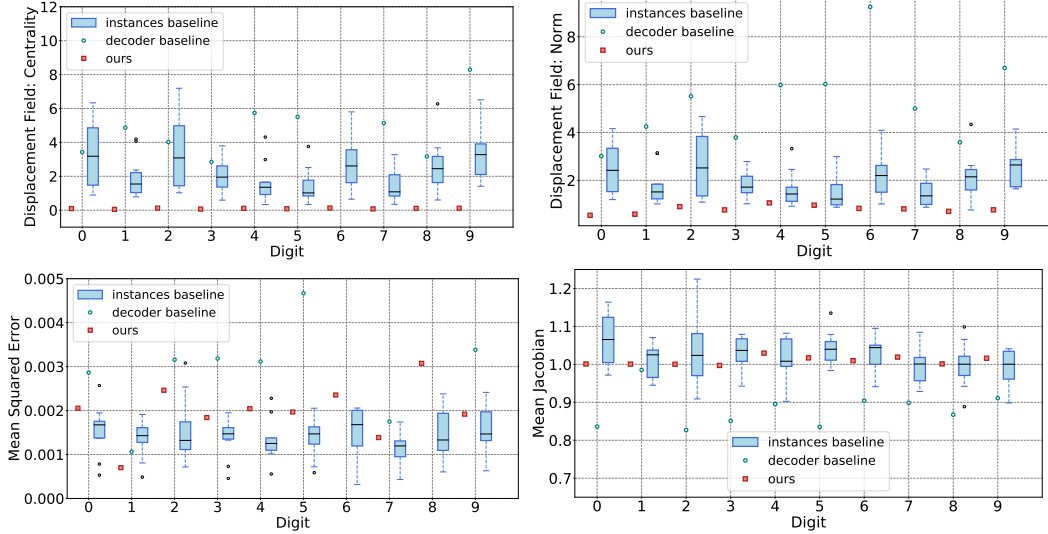


Figure 6: **Quantitative measures.** Top: Centrality and average deformation norm for templates generated by our model and the baselines on the D-class variant of MNIST. We find that our models yield more central templates. Bottom: Both MSE and Jacobians determinants measures indicate good deformations for all models.

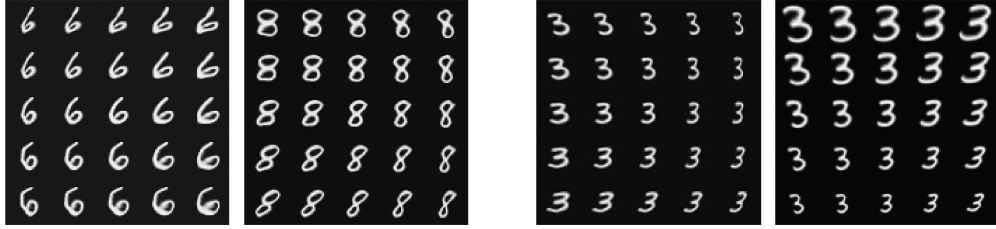


Figure 7: **Variability.** **Left:** Images are synthesized by warping a learned template from the D-class dataset along the main two axes found by applying PCA to test deformation fields. **Right:** Images are synthesized by warping learned template using the D-class-scale along the main two axes found by applying PCA. The first model uses scale as an attribute, learning mostly *other* meaningful geometric deformations. The second model does not use scale as an attribute; consequently both principal components are dominated by scale.

that changes in the hyperparameters will produce slightly different trade offs for these measures. At the presented parameters, our method produces templates and deformation fields with slightly smoother deformation fields coming at a slight cost in MSE for some digits, while the baselines can lead to slightly irregular fields to force images to match. The *decoder* baselines underperforms in all metrics. These results indicate that both our methods and instance-based templates can lead to accurate and smooth deformation fields, while our methods produce more central template requiring *smaller* deformations.

4.1.2 Analysis

In this section, we explore further characteristics and utility provided by our model using the MNIST and QuickDraw dataset.

Variability and Synthesis.

Conditional deformable templates capture an image representation up to a spatial deformation. Deformation fields from templates to images are often studied to characterize and visualize variability in a population. To illustrate this point, we demonstrate the main within-class variability by finding

0 0 0 0 0 0 0 0 0 0 0 0	0 0 0 0 0 0 0 0 0 0 0 0
1 1 1 1 1 1 1 1 1 1 1 1	1 1 1 1 1 1 1 1 1 1 1 1
2 2 2 2 2 2 2 2 2 2 2 2	2 2 2 2 2 2 2 2 2 2 2 2
3 3 3 3 3 3 3 3 3 3 3 3	3 3 3 3 3 3 3 3 3 3 3 3
4 4 4 4 4 4 4 4 4 4 4 4	4 4 4 4 4 4 4 4 4 4 4 4
5 5 5 5 5 5 5 5 5 5 5 5	5 5 5 5 5 5 5 5 5 5 5 5
6 6 6 6 6 6 6 6 6 6 6 6	6 6 6 6 6 6 6 6 6 6 6 6
7 7 7 7 7 7 7 7 7 7 7 7	7 7 7 7 7 7 7 7 7 7 7 7
8 8 8 8 8 8 8 8 8 8 8 8	8 8 8 8 8 8 8 8 8 8 8 8
9 9 9 9 9 9 9 9 9 9 9 9	9 9 9 9 9 9 9 9 9 9 9 9

Figure 8: **Missing attributes.** Left: during training, digits 3-5 are not synthesized using scaling 0.9 – 1.1. Right: during training, only 5 examples of digit 5 are given. Red boxes highlight templates build with attributes where data was held out.

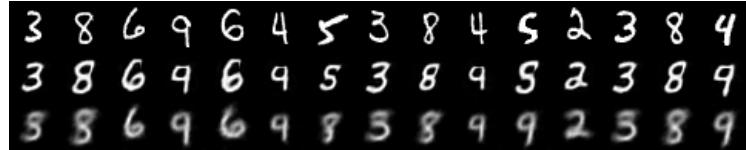


Figure 9: **Latent attribute results.** The top row shows sample input digits. The middle row shows our reconstruction for those input images, highlighting that the model learns a template for each digit type even when the digit attribute is not explicitly given. The bottom row shows templates built using an autoencoder with a single neuron bottleneck, showing that the main variation captured in this manner encourages small pixel intensity error, rather than the geometric difference minimized by our method.

the principal components of the velocity fields using PCA. Figure 7 illustrates synthesized digits by warping the template along these components capturing handwriting variability in natural digits.

In a second variability experiment, we treat *scale* as a confounder and validate that our method reduces confounding effects. Figure 7 illustrates that a model learned with a scale attribute is able to learn principal geometric variability with reduced effects from scale compared to one not using this attribute.

Missing Attributes.

We test the ability of our conditional framework to learn templates that generalize to sparsely observed attributes in two regimes. First, for the D-class-scale dataset, we completely hold out scaling factors in the range 0.9 – 1.1 for images of digits 3, 4 and 5. In the second regime, we hold out all but 5 instances of the digit 5. Figure 8 indicates that for each regime, our method produces reasonable templates even for the held out attributes, indicating that it leverages the entire dataset in learning the conditioning function.

Latent attributes.

In this experiment, we compare our method to recent probabilistic models in the situation where attributes are not known *a priori*. To do this, we add an encoder from the input image x_i to the latent attribute, and as a baseline train an autoencoder with the same encoder and decoder architectures as used in our model, and the MSE loss. We train on the D-class dataset with a bottleneck of a single neuron simulating the single unknown attribute. While more powerful autoencoders can lead to better *reconstructions* of the inputs, our goal is to explore the *main* mode of variability captured by each method. As Figure 9 shows, this autoencoder produces much fuzzier looking reconstructions, whereas our approach tends to reproduce the template for the given digit image. This is because the autoencoder learns representations to minimize pixel intensity differences, whereas our approach learns representations that minimize spatial deformations. In other words, our model learns image representations with respect to minimal geometric deformations.

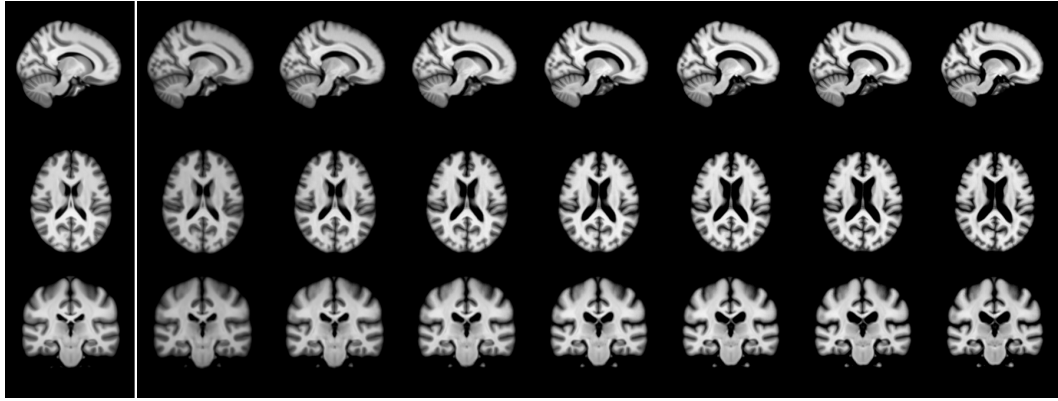


Figure 10: **Slices from Learned 3D Brain MRI templates.** Left: single unconditional template representing the entire population. Right: conditional age templates for brain MRI for ages 15 to 90, illustrating, for example, growth of the ventricles, also evident in a supplementary video.

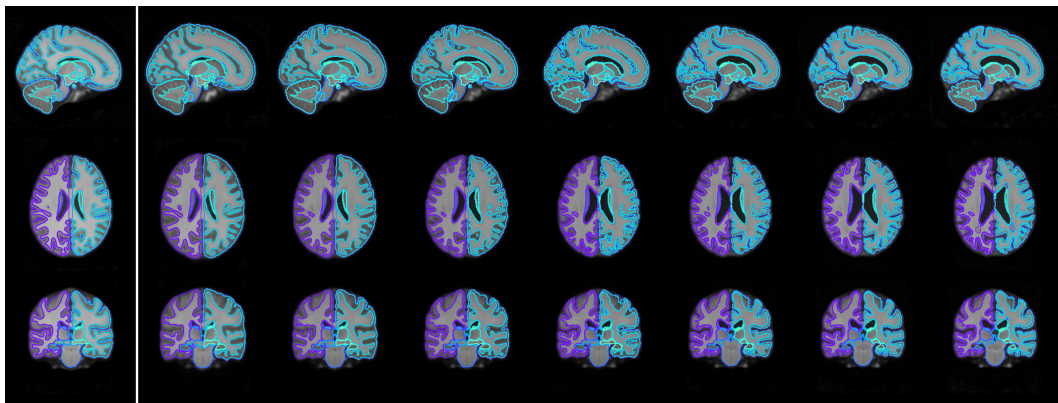


Figure 11: **Segmentations.** Example segmentations overlayed with different brain views for our unconditional template (left) and conditional templates (right) varying by age.

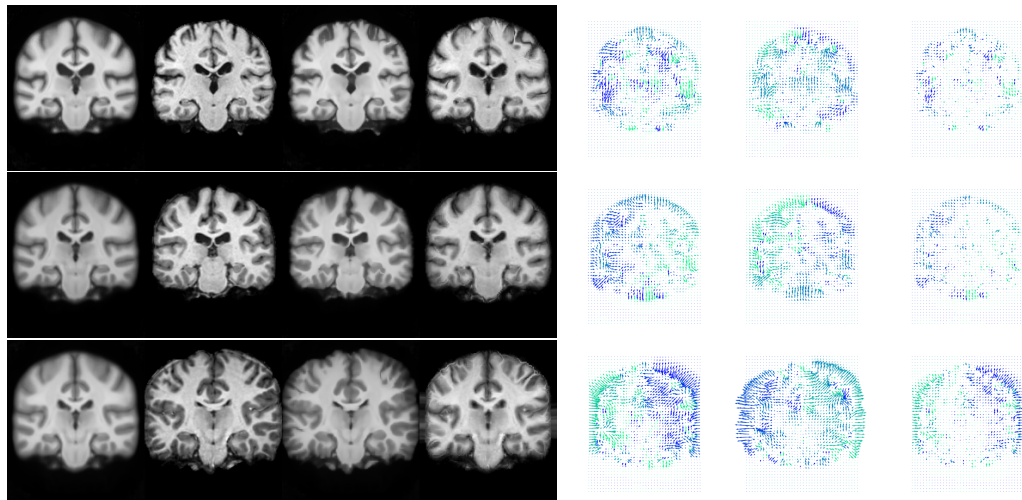


Figure 12: **Example 3D neuroimaging deformations.** Frames include: coronal slices for age-conditional template, subject scan, warped template onto subject, warped subject onto template (using inverse field), and the first two directions of the 3D forward and inverse warps, and velocity field.

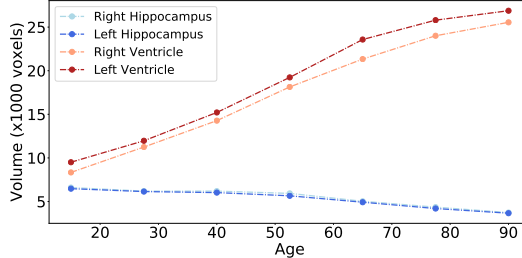


Figure 13: **Volume trends.** Change in volume of ventricles and hippocampi of the age-conditional brain templates.

4.2 Experiment 2: Neuroimaging

In this section, we illustrate unconditional and conditional 3D brain MRI templates learned by our method, with the goal of showing its utility for the realistic task of neuroimaging analysis. We first show that our method efficiently synthesizes a unconditional population template, comparable to existing ones that require significantly more computation to construct. Secondly, we show that our learned *conditional* template function captures anatomical variability as a function of age.

Data. We use a large dataset of 7829 T1-weighted 3D brain MRI scans from publicly available datasets: ADNI [58], OASIS [52], ABIDE [24], ADHD200 [54], MCIC [29], PPMI [53], HABS [16], and Harvard GSP [34]. All scans are pre-processed with standard steps, including resampling to 1mm isotropic voxels, affine spatial normalization and anatomical segmentations using FreeSurfer [27]. Final images are cropped to $160 \times 192 \times 224$. The segmentation maps are only used for analysis. The dataset is split into 7329 training volumes, 250 validation and 250 test. This dataset was first assembled and used in [20]

Methods. All of the training data was used to build an unconditional template. We also learned a conditional template function using age and sex attributes, using only the ADNI and ABIDE datasets which provide this information. Following neuroimaging literature, we use a likelihood model resulting in normalized cross correlation data loss. Training the model requires approximately a day on a Titan XP GPU. However, obtaining a conditional template from a learned network requires less than a second.

Evaluation. For a given template, we obtain anatomical segmentations by warping 100 training images to the template and averaging their warped segmentations. For the conditional template, we do this for 7 ages equally spaced between 15 and 90 years old, for both males and females. We first analyze anatomical trends with respect to conditional attributes. We then measured registration accuracy facilitated by each template with the test set via the widely used volume overlap measure Dice (higher is better). To compare volume overlap via the Dice metric, as a baseline we use the atlas and segmentation masks available online from recent literature [8]. To test the volume overlap with anatomical segmentations of test data, we warp each template (unconditional, appropriate age and sex conditional template, and baseline) to each of 100 test subjects, and propagate the template segmentations. We computed the mean Dice score of all subjects and 30 FreeSurfer labels.

Results. Figures 10 and 11, and a supplementary video², illustrate example slices from the unconditional and conditional 3D templates. The ventricles and hippocampi are known to have significant anatomical variation as a function of age, which can be seen in the images. Figure 13 illustrates their volume measured using our atlases as a function of age, showing the growth of the ventricle volumes and shrinkage of the hippocampus. Figure 12 illustrates representative results.

We find Dice scores of 0.800 (± 0.110) for the unconditional template, 0.795 (± 0.116) for the conditional model, and 0.731 (± 0.153) for the baseline, with this difference roughly consistent for each anatomical structure. We emphasize that these numbers may not be directly compared, since the baseline atlas (and segmentations) were obtained using a different process involving an external dataset and manual labeling, while our template was built with our training images (and their FreeSurfer segmentations to obtain template labels). Nonetheless, these visualizations and analyses are encouraging, suggesting that our method provides anatomical templates for brain MRI that enable brain segmentation.

²Video can be found at http://voxelmorph.mit.edu/atlas_creation/

5 Discussion and Conclusion

Deformable templates play an important role in image analysis tasks. In this paper, we present a method for automatically learning such templates from data. Our method is both less labor intensive and computationally more efficient than traditional data-driven methods for learning templates. Moreover, our method can be used to learn a function that can quickly generate templates conditioned upon sets of attributes. It can for example generate a template for the brains of 75 year old women in under a second. To our knowledge, this is the only general method for producing templates conditioned on available attributes.

In a series of experiments on popular data sets of images, we demonstrate that our method produces high quality unconditional templates. We also show that it can be used to construct conditional templates that account for confounders such as scaling and rotation. In a second set of experiments, we demonstrate the practical utility of our methods by applying it to a large data set of brain MRI images. We show that with about a day of training, we can produce unconditional atlases similar in quality and utility to a widely used atlas that took weeks to produce. We also show that the method can be used to rapidly produce conditional atlases that are consistent with known age-related changes in anatomy.

In the future, we plan to explore downstream consequences of being able to easily and quickly produce conditional templates for medical imaging studies. In addition, we believe that our model can be used for other tasks, such as estimating *unknown* attributes (e.g., age) for a given patient, which would be an interesting direction for further exploration.

References

- [1] Waleed H Abdulla, David Chow, and Gary Sin. Cross-words reference template for dtw-based speech recognition systems. In *TENCON 2003. Conference on convergent technologies for Asia-Pacific region*, volume 4, pages 1576–1579. IEEE, 2003.
- [2] Aria Ahmadi and Ioannis Patras. Unsupervised convolutional neural networks for motion estimation. In *Image Processing (ICIP), 2016 IEEE International Conference on*, pages 1629–1633. IEEE, 2016.
- [3] Stéphanie Allassonnière, Yali Amit, and Alain Trouvé. Towards a coherent statistical framework for dense deformable template estimation. *Journal of the Royal Statistical Society: Series B (Statistical Methodology)*, 69(1):3–29, 2007.
- [4] Martin Arjovsky, Soumith Chintala, and Léon Bottou. Wasserstein gan. *arXiv preprint arXiv:1701.07875*, 2017.
- [5] J. Ashburner. A fast diffeomorphic image registration algorithm. *Neuroimage*, 38(1):95–113, 2007.
- [6] Brian B Avants, Charles L Epstein, Murray Grossman, and James C Gee. Symmetric diffeomorphic image registration with cross-correlation: evaluating automated labeling of elderly and neurodegenerative brain. *Medical image analysis*, 12(1):26–41, 2008.
- [7] R. Bajcsy and S. Kovacic. Multiresolution elastic matching. *Computer Vision, Graphics, and Image Processing*, 46:1–21, 1989.
- [8] G. Balakrishnan, A. Zhao, M.R. Sabuncu, J. Guttag, and A.V. Dalca. An unsupervised learning model for deformable medical image registration. In *Proceedings of the IEEE Conference on Computer Vision and Pattern Recognition*, pages 9252–9260, 2018.
- [9] G. Balakrishnan, A. Zhao, M.R. Sabuncu, J. Guttag, and A.V. Dalca. Voxelmorph: A learning framework for deformable medical image registration. *IEEE Transactions on Medical Imaging*, 2018.
- [10] M.F. Beg et al. Computing large deformation metric mappings via geodesic flows of diffeomorphisms. *Int. J. Comput. Vision*, 61:139–157, 2005.
- [11] Thomas Brox et al. High accuracy optical flow estimation based on a theory for warping. *European Conference on Computer Vision (ECCV)*, pages 25–36, 2004.
- [12] Xiaohuan Cao, Jianhua Yang, Jun Zhang, Dong Nie, Minjeong Kim, Qian Wang, and Dinggang Shen. Deformable image registration based on similarity-steered cnn regression. In *International*

Conference on Medical Image Computing and Computer-Assisted Intervention, pages 300–308. Springer, 2017.

- [13] Yan Cao, Michael I Miller, Raimond L Winslow, and Laurent Younes. Large deformation diffeomorphic metric mapping of vector fields. *IEEE transactions on medical imaging*, 24(9):1216–1230, 2005.
- [14] Can Ceritoglu, Kenichi Oishi, Xin Li, Ming-Chung Chou, Laurent Younes, Marilyn Albert, Constantine Lyketsos, Peter CM van Zijl, Michael I Miller, and Susumu Mori. Multi-contrast large deformation diffeomorphic metric mapping for diffusion tensor imaging. *Neuroimage*, 47(2):618–627, 2009.
- [15] Xi Chen, Yan Duan, Rein Houthooft, John Schulman, Ilya Sutskever, and Pieter Abbeel. Infogan: Interpretable representation learning by information maximizing generative adversarial nets. In *Advances in neural information processing systems*, pages 2172–2180, 2016.
- [16] A. Dagley et al. Harvard aging brain study: dataset and accessibility. *NeuroImage*, 2015.
- [17] A.V. Dalca, G. Balakrishnan, J. Guttag, and M.R. Sabuncu. Unsupervised learning for fast probabilistic diffeomorphic registration. In *International Conference on Medical Image Computing and Computer-Assisted Intervention*, pages 729–738. Springer, 2018.
- [18] A.V. Dalca, G. Balakrishnan, J. Guttag, and M.R. Sabuncu. Unsupervised learning of probabilistic diffeomorphic registration for images and surfaces. *Medical Image Analysis*, 57:226–236, 2019.
- [19] A.V. Dalca et al. Patch-based discrete registration of clinical brain images. In *International Workshop on Patch-based Techniques in Medical Imaging*, pages 60–67. Springer, 2016.
- [20] A.V. Dalca, J. Guttag, and M.R. Sabuncu. Anatomical priors in convolutional networks for unsupervised biomedical segmentation. In *Proceedings of the IEEE Conference on Computer Vision and Pattern Recognition*, pages 9290–9299, 2018.
- [21] Brad Davis, Peter Lorenzen, and Sarang C Joshi. Large deformation minimum mean squared error template estimation for computational anatomy. In *ISBI*, volume 4, pages 173–176, 2004.
- [22] Brad C Davis, P Thomas Fletcher, Elizabeth Bullitt, and Sarang Joshi. Population shape regression from random design data. *International journal of computer vision*, 90(2):255–266, 2010.
- [23] B.D. de Vos et al. End-to-end unsupervised deformable image registration with a convolutional neural network. In *DLMIA*, pages 204–212. 2017.
- [24] A. Di Martino et al. The autism brain imaging data exchange: towards a large-scale evaluation of the intrinsic brain architecture in autism. *Molecular psychiatry*, 19(6):659–667, 2014.
- [25] A. Dosovitskiy et al. Flownet: Learning optical flow with convolutional networks. 2015.
- [26] Pedro F Felzenszwalb and Joshua D Schwartz. Hierarchical matching of deformable shapes. In *2007 IEEE Conference on Computer Vision and Pattern Recognition*, pages 1–8. IEEE, 2007.
- [27] B. Fischl. Freesurfer. *Neuroimage*, 62(2):774–781, 2012.
- [28] Ben Glocker et al. Dense image registration through mrf’s and efficient linear programming. *Medical image analysis*, 12(6):731–741, 2008.
- [29] R.L. Gollub et al. The mcic collection: a shared repository of multi-modal, multi-site brain image data from a clinical investigation of schizophrenia. *Neuroinformatics*, 11(3):367–388, 2013.
- [30] Ian Goodfellow, Yoshua Bengio, and Aaron Courville. *Deep learning*. MIT Press, 2016.
- [31] Piotr A Habas, Kio Kim, Francois Rousseau, Orit A Glenn, A James Barkovich, and Colin Studholme. A spatio-temporal atlas of the human fetal brain with application to tissue segmentation. In *International Conference on Medical Image Computing and Computer-Assisted Intervention*, pages 289–296. Springer, 2009.
- [32] Monica Hernandez, Matias N Bossa, and Salvador Olmos. Registration of anatomical images using paths of diffeomorphisms parameterized with stationary vector field flows. *International Journal of Computer Vision*, 85(3):291–306, 2009.

[33] Irina Higgins, Loic Matthey, Arka Pal, Christopher Burgess, Xavier Glorot, Matthew Botvinick, Shakir Mohamed, and Alexander Lerchner. beta-vae: Learning basic visual concepts with a constrained variational framework. *ICLR*, 2(5):6, 2017.

[34] A. J Holmes et al. Brain genomics superstruct project initial data release with structural, functional, and behavioral measures. *Scientific data*, 2, 2015.

[35] Berthold K.P. Horn and Brian G. Schunck. Determining optical flow. 1980.

[36] Eddy Ilg, Nikolaus Mayer, Tonmoy Saikia, Margret Keuper, Alexey Dosovitskiy, and Thomas Brox. Flownet 2.0: Evolution of optical flow estimation with deep networks. In *IEEE conference on computer vision and pattern recognition (CVPR)*, volume 2, page 6, 2017.

[37] Anil K. Jain, Yu Zhong, and Sridhar Lakshmanan. Object matching using deformable templates. *IEEE Transactions on pattern analysis and machine intelligence*, 18(3):267–278, 1996.

[38] J Yu Jason, Adam W Harley, and Konstantinos G Derpanis. Back to basics: Unsupervised learning of optical flow via brightness constancy and motion smoothness. In *European Conference on Computer Vision*, pages 3–10. Springer, 2016.

[39] Jonas Jongejan, Henry Rowley, Takashi Kawashima, Jongmin Kim, and Nick Fox-Gieg. The quick, draw!-ai experiment. *Mount View, CA, accessed Feb*, 17:2018, 2016.

[40] Sarang Joshi, Brad Davis, Matthieu Jomier, and Guido Gerig. Unbiased diffeomorphic atlas construction for computational anatomy. *NeuroImage*, 23:S151–S160, 2004.

[41] Sarang C Joshi and Michael I Miller. Landmark matching via large deformation diffeomorphisms. *IEEE transactions on image processing*, 9(8):1357–1370, 2000.

[42] Jaechul Kim, Ce Liu, Fei Sha, and Kristen Grauman. Deformable spatial pyramid matching for fast dense correspondences. In *Proceedings of the IEEE Conference on Computer Vision and Pattern Recognition*, pages 2307–2314, 2013.

[43] D.P. Kingma and M. Welling. Auto-encoding variational bayes. *ICLR*, 2014.

[44] Iasonas Kokkinos, Michael M Bronstein, Roee Litman, and Alex M Bronstein. Intrinsic shape context descriptors for deformable shapes. In *2012 IEEE Conference on Computer Vision and Pattern Recognition*, pages 159–166. IEEE, 2012.

[45] J. Krebs, T. Mansi, B. Mailhé, N. Ayache, and H. Delingette. Unsupervised probabilistic deformation modeling for robust diffeomorphic registration. *Deep Learning in Medical Image Analysis*, 2018.

[46] Julian Krebs, Hervé Delingette, Boris Mailhé, Nicholas Ayache, and Tommaso Mansi. Learning a probabilistic model for diffeomorphic registration. *IEEE transactions on medical imaging*, 2019.

[47] Julian Krebs et al. Robust non-rigid registration through agent-based action learning. In *Medical Image Computing and Computer-Assisted Intervention (MICCAI)*, pages 344–352, Cham, 2017. Springer International Publishing.

[48] Maria Kuklisova-Murgasova, Paul Aljabar, Latha Srinivasan, Serena J Counsell, Valentina Doria, Ahmed Serag, Ioannis S Gousias, James P Boardman, Mary A Rutherford, A David Edwards, et al. A dynamic 4d probabilistic atlas of the developing brain. *NeuroImage*, 54(4):2750–2763, 2011.

[49] Yann LeCun. The mnist database of handwritten digits. <http://yann.lecun.com/exdb/mnist/>, 1998.

[50] Jun Ma, Michael I Miller, Alain Trouvé, and Laurent Younes. Bayesian template estimation in computational anatomy. *NeuroImage*, 42(1):252–261, 2008.

[51] Alireza Makhzani, Jonathon Shlens, Navdeep Jaitly, Ian Goodfellow, and Brendan Frey. Adversarial autoencoders. *arXiv preprint arXiv:1511.05644*, 2015.

[52] D.S. Marcus et al. Open access series of imaging studies (oasis): cross-sectional mri data in young, middle aged, nondemented, and demented older adults. *Journal of cognitive neuroscience*, 19(9):1498–1507, 2007.

[53] K. Marek et al. The parkinson progression marker initiative (ppmi). *Progress in neurobiology*, 95(4):629–635, 2011.

[54] M.P. Milham et al. The adhd-200 consortium: a model to advance the translational potential of neuroimaging in clinical neuroscience. *Front. Sys. Neurosci*, 6:62, 2012.

[55] Michael I Miller, M Faisal Beg, Can Ceritoglu, and Craig Stark. Increasing the power of functional maps of the medial temporal lobe by using large deformation diffeomorphic metric mapping. *Proceedings of the National Academy of Sciences*, 102(27):9685–9690, 2005.

[56] M. Modat, I.J.A. Simpson, M.J. Cardoso, D.M. Cash, N. Toussaint, N.C. Fox, and S. Ourselin. Simulating neurodegeneration through longitudinal population analysis of structural and diffusion weighted mri data. *Medical Image Computing and Computer-Assisted Intervention, LNCS* 8675:57–64, 2014.

[57] Marc Modat, Pankaj Daga, M Jorge Cardoso, Sebastien Ourselin, Gerard R Ridgway, and John Ashburner. Parametric non-rigid registration using a stationary velocity field. In *2012 IEEE Workshop on Mathematical Methods in Biomedical Image Analysis*, pages 145–150. IEEE, 2012.

[58] S.G. Mueller et al. Ways toward an early diagnosis in Alzheimer’s disease: the Alzheimer’s Disease Neuroimaging Initiative (ADNI). *Alzheimer’s & Dementia*, 1(1):55–66, 2005.

[59] Kenichi Oishi, Andreia Faria, Hangyi Jiang, Xin Li, Kazi Akhter, Jiangyang Zhang, John T Hsu, Michael I Miller, Peter CM van Zijl, Marilyn Albert, et al. Atlas-based whole brain white matter analysis using large deformation diffeomorphic metric mapping: application to normal elderly and alzheimer’s disease participants. *Neuroimage*, 46(2):486–499, 2009.

[60] Anurag Ranjan and Michael J Black. Optical flow estimation using a spatial pyramid network. In *IEEE Conference on Computer Vision and Pattern Recognition (CVPR)*, volume 2, page 2. IEEE, 2017.

[61] M.M. Rohé et al. SVF-Net: Learning deformable image registration using shape matching. In *MICCAI*, pages 266–274. Springer, 2017.

[62] O. Ronneberger et al. U-net: Convolutional networks for biomedical image segmentation. In *MICCAI*, pages 234–241. Springer, 2015.

[63] Mert R Sabuncu, Serdar K Balci, Martha E Shenton, and Polina Golland. Image-driven population analysis through mixture modeling. *IEEE transactions on medical imaging*, 28(9):1473–1487, 2009.

[64] H. Sokooti et al. Nonrigid image registration using multi-scale 3d convolutional neural networks. In *MICCAI*, pages 232–239, Cham, 2017. Springer.

[65] Carsten Stoll, Zachi Karni, Christian Rössl, Hitoshi Yamauchi, and Hans-Peter Seidel. Template deformation for point cloud fitting. In *SPBG*, pages 27–35, 2006.

[66] D. Sun et al. Secrets of optical flow estimation and their principles. *IEEE Conf. on Computer Vision and Pattern Recognition (CVPR)*, pages 2432–2439, 2010.

[67] J.P. Thirion. Image matching as a diffusion process: an analogy with maxwell’s demons. *Medical Image Analysis*, 2(3):243–260, 1998.

[68] Du Tran, Lubomir Bourdev, Rob Fergus, Lorenzo Torresani, and Manohar Paluri. Deep end2end voxel2voxel prediction. In *Proceedings of the IEEE Conference on Computer Vision and Pattern Recognition Workshops*, pages 17–24, 2016.

[69] Tom Vercauteren et al. Diffeomorphic demons: Efficient non-parametric image registration. *NeuroImage*, 45(1):S61–S72, 2009.

[70] X. Yang et al. Quicksilver: Fast predictive image registration—a deep learning approach. *NeuroImage*, 158:378–396, 2017.

[71] BT Thomas Yeo, Mert R Sabuncu, Tom Vercauteren, Daphne J Holt, Katrin Amunts, Karl Zilles, Polina Golland, and Bruce Fischl. Learning task-optimal registration cost functions for localizing cytoarchitecture and function in the cerebral cortex. *IEEE transactions on medical imaging*, 29(7):1424–1441, 2010.

[72] Aras Yurtman and Billur Barshan. Automated evaluation of physical therapy exercises using multi-template dynamic time warping on wearable sensor signals. *Computer methods and programs in biomedicine*, 117(2):189–207, 2014.

[73] M. Zhang et al. Frequency diffeomorphisms for efficient image registration. In *IPMI*, pages 559–570. Springer, 2017.

1 Architectures.

We model the conditional template network architecture as a decoder with a dense layer followed by several upsampling and convolutional levels. Class attributes are encoded as one-hot representations, and continuous attributes are encoded as scalars. For toy datasets, we use a dense layer from the input attributes to a 4×4 image with k features followed by three upsampling levels with two convolution layers each with 16 features each. The value for k is set to 8 in most situations, and in the latent variable experiment, we avoid over-fitting by using a bottleneck of 1 and k of 2, for both our method and the baseline. Unconditional templates involve a single layer with a learnable parameter at each pixel.

For our conditional 3D neuroimaging template, we use a dense layer to a $80 \times 96 \times 112$ 3D image with 8 features, followed by a level of upsampling with three convolution layers and 8 features. All kernels are of size 3.

We base our design for the registration network on the architecture described in recent learning-based registration frameworks [9]. Specifically, we use a U-Net style architecture with four downsampling and upsampling layers, each involving a convolutional layer with 32 features and 3x3 kernel size. This is followed by two more convolution layers. For baseline templates – instances, and those produced by decoder-based models – we learn a registration network using the same architecture.

2 Quickdraw result examples

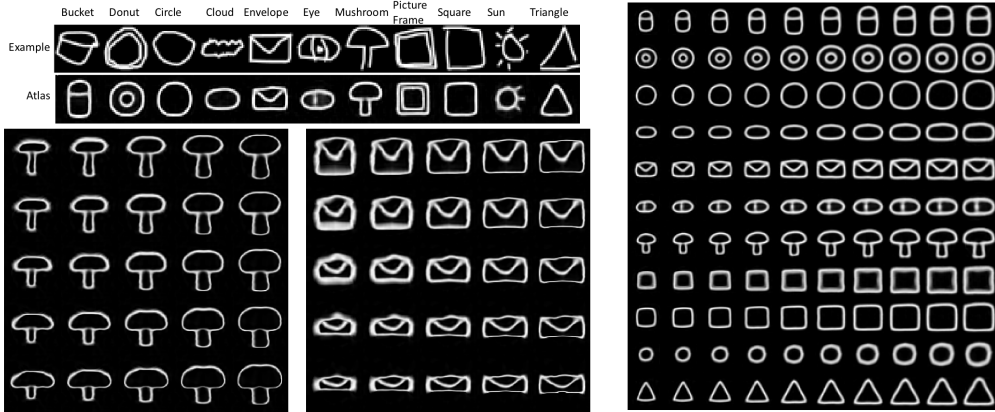


Figure 14: **Quickdraw example templates.** Left: example and learned atlases for the D-class QuickDraw dataset, and below variability examples similar to Figure 7-left. Right: templates for different scales and classes learned using D-class-scale simulations.

3 Supplementary Video

We include a supplementary video at http://voxelmorph.mit.edu/atlas_creation/, illustrating our method’s ability of synthesizing templates on-demand based on given attributes. Specifically, the video illustrates the brain template conditioned on age, between 15 and 90 years old, also used as the video frame index.